4.5 2D PIV Measurements of Street Canyon Flow for Buildings with Varying Angles and Separation Distances

Bhagirath Addepalli, Eric R. Pardyjak - University of Utah

1. INTRODUCTION

The objective of the present work is to try to better understand the mechanisms that govern the transport of pollutants in a street canyon through wind tunnel experiments to help improve dispersion modeling work. To this end, 2D PIV was used to study the flow in a street canyon. Velocity and turbulence statistics were obtained along the center plane of the model buildings. A number of studies in the past have researched the flow in a street canyon through wind tunnel experiments – Hoydysh & Dabberdt 1988, Kastner-Klein & Rotach 2004, Kastner-Klein, Berkowicz & Britter 2004, through analytical models - Hotchkiss, & Harlow 1973, and through numerical models and simulations - Hunter et al 1992, Cheng & Hu 2005. Though extensive literature can be found for the cases of street canyons with varying building heights to the width of the street canyon (H/W) ratios, very little work has been done for the case of a street canyon with the orientation of the buildings in the street canyon varied with respect to one another and to the approaching boundary layer. The present work is an endeavor to understand the flow field when the model buildings are at and angle to the approaching boundary layer.

The transport of pollutants in a street canyon depends upon umpteen parameters and for the present experiment, two such parameters; namely, the distances between the buildings (x) and the alignment of the buildings to the approaching boundary layer (α and β) have been varied and their effect upon the flow field in the street canyon has been studied. Though the experiments were performed for two different street canyon widths(W = x =3.5H and 4H) with the upwind and downwind buildings at different angles, only the results for the case where the upwind building was rotated with respect to the approaching boundary layer have been presented in this paper.

Hussain & Lee 1980 proposed that for a street canyon normal to the approaching boundary layer, the value of H/W determines the type of flow in a street canyon (isolated roughness flow, wake interference or skimming flow). In the present paper, an effort is made to understand the significance and relevance of the value of H/W for the various configurations being investigated. Future work will involve stereoscopic PIV measurements at planes other than the centerline and should help explain the onset of channeling as a function of the spanwise component of velocity for the configurations being considered.

2. EXPERIMENTAL METHOD

2.1 Flow conditions and setup

The experiments were performed in the Physical Fluid Dynamics Laboratory at the University of Utah at an atmospheric pressure of 648.5mm of Hg, temperature of 21.5°C in a 7.9 m long boundary layer wind tunnel facility having a working cross section of 0.61m × 0.91 m. The free stream velocity was ~ 7 m/s and the boundary layer exponent was ~ 0.23.

2.2 Canyon Models and Configurations

Cubes of side dimension 32mm were used to model the buildings of the street canyon. Lego sheets of height 2mm lined the floor of the wind tunnel and were used to model small scale roughness elements. They were used to produce uniform rough walled turbulent flow.

2.2.1 Notation

The following notation will be used to address the different canyon configurations considered for the experiment throughout the course of this paper.

H = height of the buildings
α = angle by which the upwind building is rotated with respect to the approaching boundary layer (counterclockwise)
β = angle by which β-building is rotated with respect to the approaching boundary layer (counterclockwise)
x = streamwise distance between the centers of the buildings in terms of H
z = vertical distance above the ground.

X = distance of a given profile from the center of the upwind building

An example using this notation would be for case: x4H_ α15_15β. This would represent the street canyon configuration with the buildings separated by x = 4H (center to center distance), with the upwind building set at an angle of 15^o to the approaching boundary layer and the downwind building at and angle of 15^o to the boundary layer.

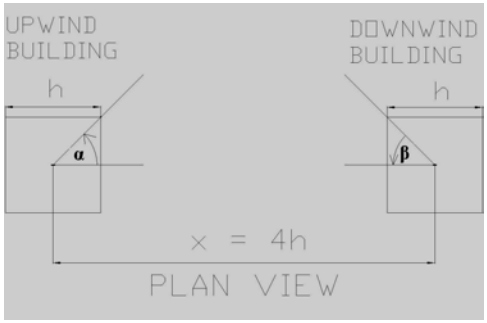

Figure 1 – Schematic of the street canyon flow configuration.

2.2.2 Configurations

Table 1 describes the configurations considered for measurements taken along the center plane.

Table 1 - Matrix of the various upwind and downwind buildings configurations.

x	α	β	α	β	α and β
3.5h	15,30,45	0	0	15,30,45	15,15;30,30;45,45
4h	15,30,45	0	0	15,30,45	15,15;30,30;45,45

2.3 PIV Technique

Particle Image Velocimetry (PIV) was used to obtain the temporally averaged velocity fields for the various configurations of the street canyon considered. The various aspects and parameters chosen for the technique are briefly described in the following sections.

2.3.1 Flow seeding

The flow was seeded with Olive oil particles generated using Laskin Nozzles. Two Laskin Nozzles, each operating at a pressure of ~ 80psi were used to generate the oil particles**.**

2.3.2 Seed Particle Illumination

The smoke particles were illuminated with a 532nm wavelength laser sheet generated using a 50mJ NewWave Research (Fremont, CA) Solo PIV III Nd-Yag Laser. The thickness of the laser sheet at half the street canyon height was ~ 1.5mm and this was obtained using a combination of cylindrical and spherical lenses. A 500m focal length spherical lens was used to obtain the desired light sheet thickness at the region of interest. Cylindrical lenses having focal lengths of -25mm and -50mm were used in conjunction to diverge the light sheet over the area of interest.

2.3.4 Image Acquisition

A 4.0MP (2048×2048pixels) CCD camera manufactured by TSI Inc. (Shoreview, MN) having a frame rate of 17fps was used in conjunction with a frame grabber for image acquisition. A LASERPULSE synchronizer was used to control the timing between the laser pulses and the camera shutter open time through a PC desktop computer. For the experiment, a shutter open time of 230μs was chosen for the camera, the pulse delay was set to 0.25ms and the pulse repetition rate was set to 7.5 Hz through the synchronizer. The pulse separation values (dT) for the laser for the configurations considered can be found in Table 2.

During image acquisition, reflection coming off the surface due to the incident laser light sheet often shows up as saturation in the images. Due to this, much of the data close to the surface is lost and accounts for bad correlations during image processing. Discrete roughness elements such as Legos increase the reflection coming off the surface. The presence or non-presence of Legos in between the buildings does not markedly affect the value of z_0 of the boundary layer. Therefore, the area covered by the Lego's in the street canyon (H×x) was removed and the surface was made flat to mitigate the problem of saturation in the images. The flat surface was made out of mirror that had a fluorescent covering on top and a 532nm band pass filter (± 10nm bandwidth) manufactured by LaVision was mounted on the camera lens to filter out the reflected light coming off the surface. This allowed for significant improvement of near surface image processing.

Also, to reduce the effect of saturation in the images on the building roof top and edges, red reflective tape was put over the model buildings.

2.3.5 PIV Analysis

Analysis of the acquired image pairs was done using TSI INSIGHT6 analysis software.

In order to obtain better results, background image processing was performed prior to final analysis of the images. For this, 25 sets of images were taken for the cases in Table1 replicating the experimental conditions without the seeding. 'Maximum Background Processor' was used to find over the sequence of images and over each pixel, the maximum intensity of the pixels. The analysis software then constructs an image pair with these maximum pixel intensities. The obtained image pair having the maximum pixel intensities without the seeding particles was subtracted from the images with the seeding particles. This procedure improves the SNR ratio as cross-correlation of the images is performed based on the light scattered by only the seeding particles with the background noise due to reflection and scattering from the other sources eliminated.

FFT based cross-correlation analysis was performed on the conditioned image pairs by dividing them into 32×32 pixel interrogation regions. For the present experiment, a 'Recursive Nyquist Grid' was used as the 'Grid Engine' to process the images in multiple passes. The advantage of using the 'Recursive Nyquist Grid' over a single pass Nyquist grid is that that the second pass uses the optimized window offsets to re-compute the vector field with the same number of vectors. It was found that this procedure reduced the number of bad vectors obtained and hence was employed. 600 image pairs across 12 experiments were used to get the mean and turbulence statistics for the case x = 4H and 300 image pairs across 10 experiments were used to obtain the statistics for the case x = 3.5H. The spatial resolution obtained for each case is specified in Table 2. Greater than 92% valid vectors were obtained and the remaining were removed and replaced with interpolated values. A standard deviation of 3 and tolerance value of 2 for the mean and median was chosen during the process of vector validation. No smoothing of the velocity fields was done.

Table 2 – Details of the PIV set-up parameters.

Case	Combination of cylindrical lenses on laser(mm)	dT (μs)	Focal length of camera lens (mm)	F-value on the lens	Distance between camera and area of interest(mm)	Area viewed by the camera(mm^2)	Calibration factor (in x and z) (μm/pixel)	Spatial resolution (in x and z) (mm)
x=4H	-25, -50	70	50	1.2	405	128.5×128.5	62.8	1.0
x=3.5H	-25, -50	64	50	1.2	375	120.9×120.9	59.0	0.94

Note – The distance between the camera and area of interest is the distance from the filter on the camera to the Laser sheet

3. RESULTS AND DISCUSSION

3.1 Mean Velocity Characteristics

Figures 1 to 8 show stream-traces for both the x/H= 3.5 and x/H=4.0 cases as the upwind building is rotated from normal to 45 degrees. For the cases shown, the downwind building is always normal to the incident flow.

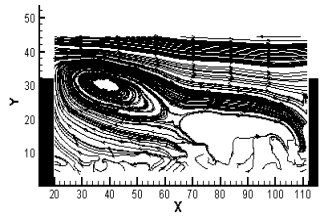

Figure 1 - x4H_ α0_0β

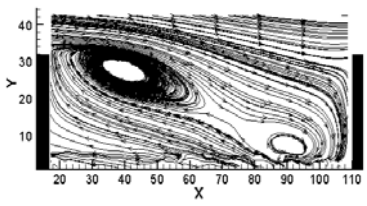

Figure 2 - x4H_ α15_0β

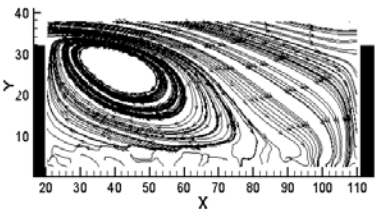

Figure 3 - x4h_ α30_0β

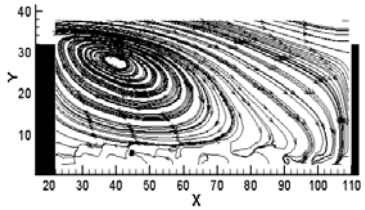

Figure 4 - x4h_ α45_0β

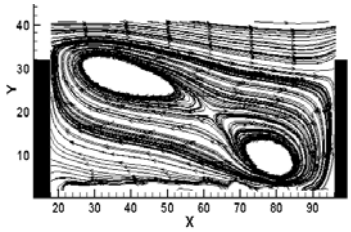

Figure 5 - x3.5h_ α0_0β

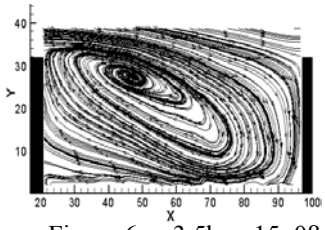

Figure 6 - x3.5h_ α15_0β

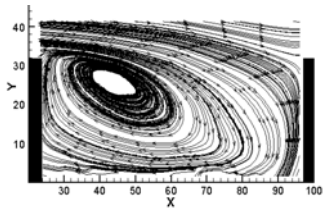

Figure 7 - x3.5h_ α30_0β

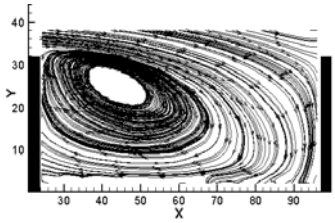

Figure 8 – x3.5h_ α45_0β

The above stream traces were obtained from the averaged velocity vector fields. On inspecting the figures we find that the data close to the surface is sparse and this is due to the inability of the seeding used in the PIV technique to entrain effectively into the boundary layer close to the surface.

Observing the transition of the mean flow field in the canyon for these cases, we find that the value of H / x for each of these cases is 0.25 and 0.29 respectively. According the work of Hussain and Lee 1980, for a normal street canyon, a value of H/W < 0.4 results in an isolated roughness flow in the street canyon. For the present cases, when the buildings are normal, the value of H/W is 0.33 and 0.25. But we do not observe an isolated flow for either of the cases. This raises a question whether H/W<0.4 is a sufficient condition for an isolated flow in a street canyon and contributes for future work on this aspect.

Also, we find that even for H/W = 0.33, the flow replicates the 'wake interference regime' more than the 'isolated flow regime' and we observe either one or two co-rotating vortices in all the figures. The flow field observed in these cases is consistent with the development of the 'wake interference regime' as simulated by Sini et al. (1996). For an infinitely wide street canyon oriented normal to the flow, they found that the wake interference regime can be described by a single main vortex that extends from the leeward wall to the downwind wall for 0.2 < H/W < 0.67. At smaller H/W (0.1 < H/W < 0.2), the vortex splits into two co-rotating vortices that slowly separate into an isolated flow**.** The present experiment confirms the observation made by Sini et al. (1996) based on their numerical model and future work would involve trying to narrow down on the interval suggested in their work.

The above figures also suggest that the flow regimes are particularly sensitive to angular orientation. As the building orientation is changed from 0 to 45°, the wake vortex of the upwind building and the upwind vortex of the downwind building merge into a single vortex and for the case when H/x = 0.29, the flow resembles the 'skimming flow regime' for a normal street canyon. This is illustrated in the vector field in Figure 9. That is, with very little change in distance between the two buildings the flow transitions from wake interference flow to skimming flow.

Also, looking at the statistics of the vertical component of velocity close to the downwind building for the street canyon with width 4H, it was observed that as the upwind building orientation was changed from 15 to 45 °, the vertical component of velocity increased from about 25% to as much as 40% of the value of the velocity at the building height in an uninterrupted boundary layer (U_H) without the

buildings. This indicates that even though the effective width of the canyon was 0.4 (which according to the work of Hussain and Lee (1980) is the threshold where we could expect an isolated flow in a normal street canyon), changing the orientation of the upwind building has a significant effect on the transport of pollutants in the street canyon near the downwind building.

3.2 TURBULENCE STATISTICS

3.2.1 Normalized TKE

Figures 10 to 13 show the behavior of normalized TKE at different equidistant locations in the street canyon for the street canyon width x = 4H.

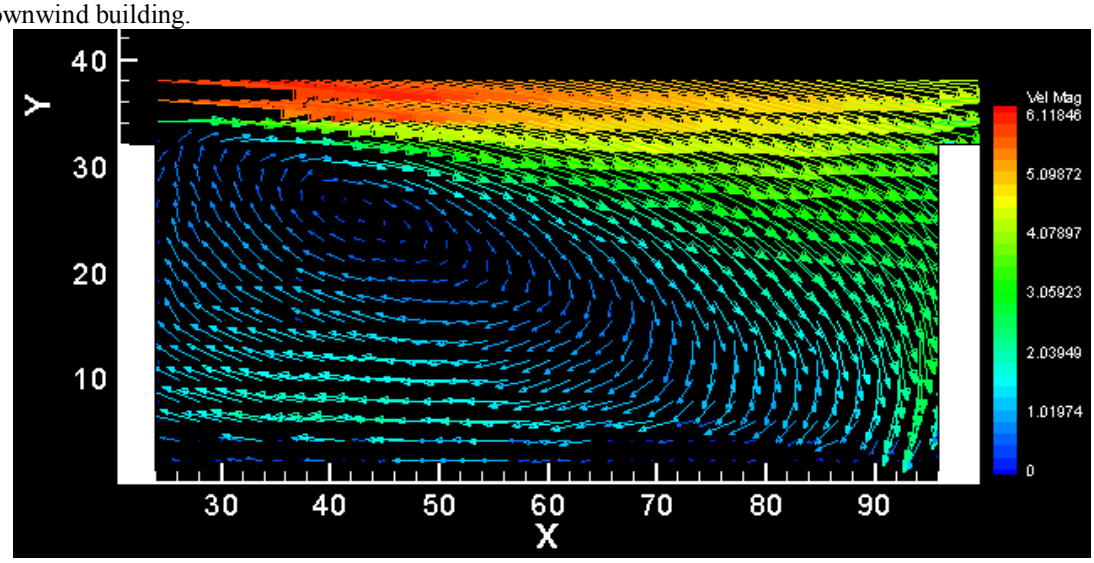

Figure 9 – Average Vector Field along the building centerline plane for the case x3.5h_ α45_0β.

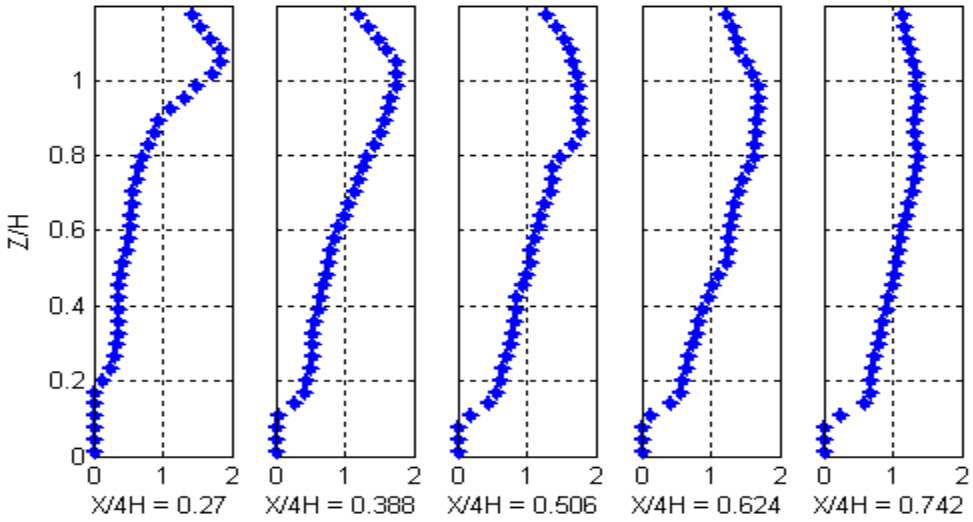

Figure 10 – Profiles of normalized TKE (TKE/$0.5U_H^2$) at five equidistant streamwise locations along the center plane of the street canyon for the x4h_α15_0β case.

Note: X/4H is the non dimensional distance of the of the location where the profile has been plotted from the center of the upwind building

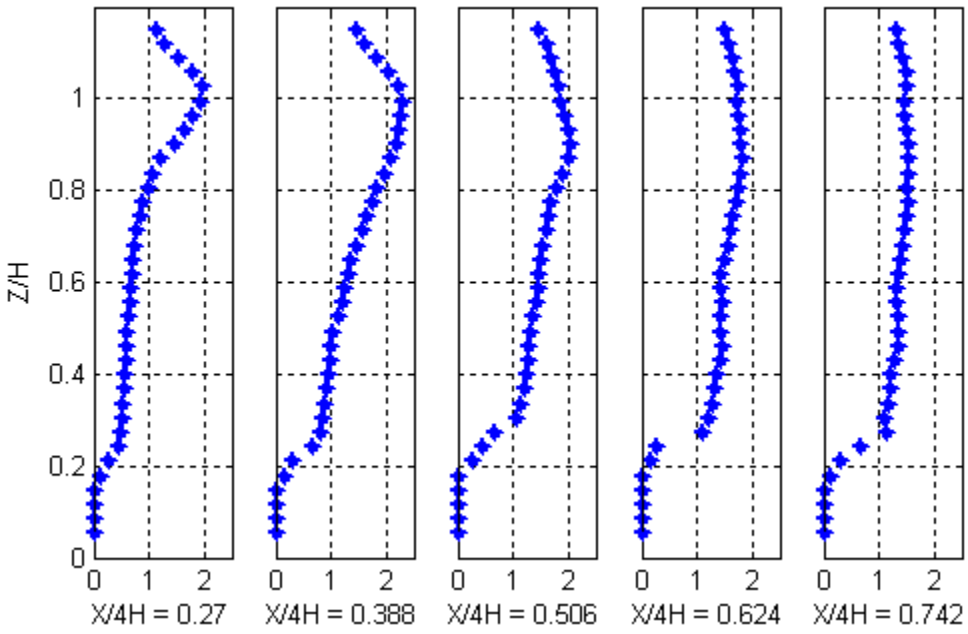

Figure 11 – Profiles of normalized TKE (TKE/$0.5U_H^2$) at five equidistant streamwise locations along the center plane of the street canyon for the x4h_α30_0β case.

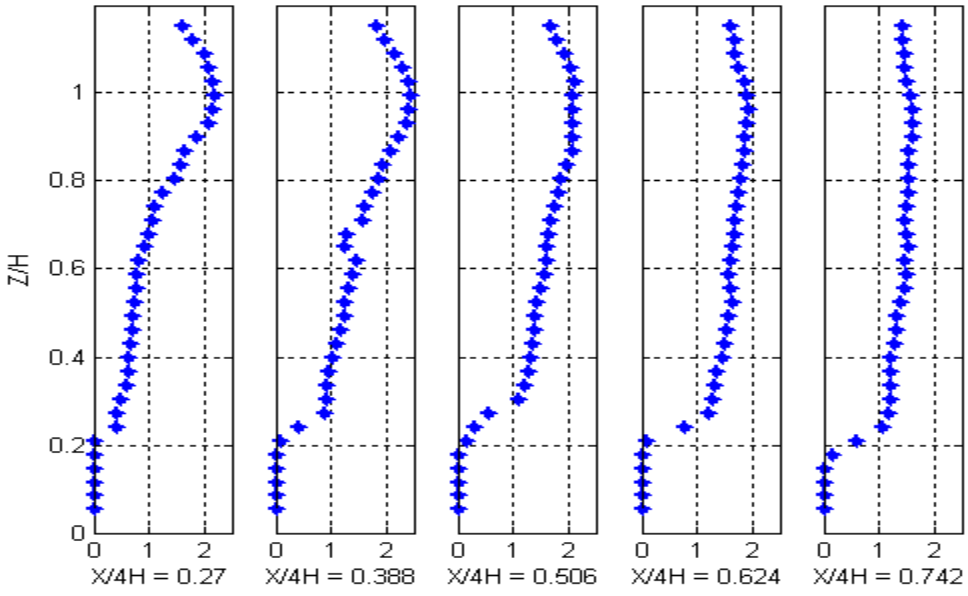

Figure 12 – Profiles of normalized TKE (TKE/$0.5U_H^2$) at five equidistant streamwise locations along the center plane of the street canyon for the x4h_α45_0β case.

Note: X/4H is the non dimensional distance of the of the location where the profile has been plotted from the center of the upwind building.

The local values of TKE have been normalized by $0.5U_H^2$, where U_H is the velocity of the boundary layer at height H in the absence of buildings. The plots indicate that the maximum value of TKE occurs almost at the building height in the shear layer.

For the cases where α = 30 and 45°, the magnitude of the maximum value is higher and occurs further downstream of the upwind building for the given locations when compared to α = 15° This effect could be possibly attributed to the fact that as the angle increases, the effective cross sectional area of the building as seen by the incoming flow increases which produces a larger and stronger wake.

3.2.2 Normalized Reynolds Stress

Figures 13 to 15 show the behavior of the normalized Reynolds stress ($\overline{u'w'}/\overline{u'w'}_H$) at different locations in the street canyon for the configuration with street canyon width x = 4H. The local values of the Reynolds stress have been normalized by the value of Reynolds Stress at the building height for each of the locations. Similar to normalized TKE, the normalized Reynolds stress is maximum at approximately the building height and diffuses downward with the development of the shear layer associated with the flow separating from the upwind building.

As was the case with normalized TKE, even the normalized Reynolds Stress has a higher magnitude for a given location for the cases α = 30° and 45° respectively.

3.2.3 Ratio of turbulent kinetic energy to Reynolds stress

Figures 16 to 18 show the behavior of the ratio TKE to the Reynolds stress for the street canyon configuration with width x = 4H. It should be noted that the data below z/H~0.2 is relatively sparse and not very reliable. The plot suggests that the ratio of TKE $/-\overline{u'w'}$ increases as we approach the surface and decreases as we approach the building height. This indicates that although relatively large turbulent fluctuations exist as the surface is approached, they are relatively uncorrelated. The magnitude at the building height was found to be ~ 1.5 for the case α = 15°.

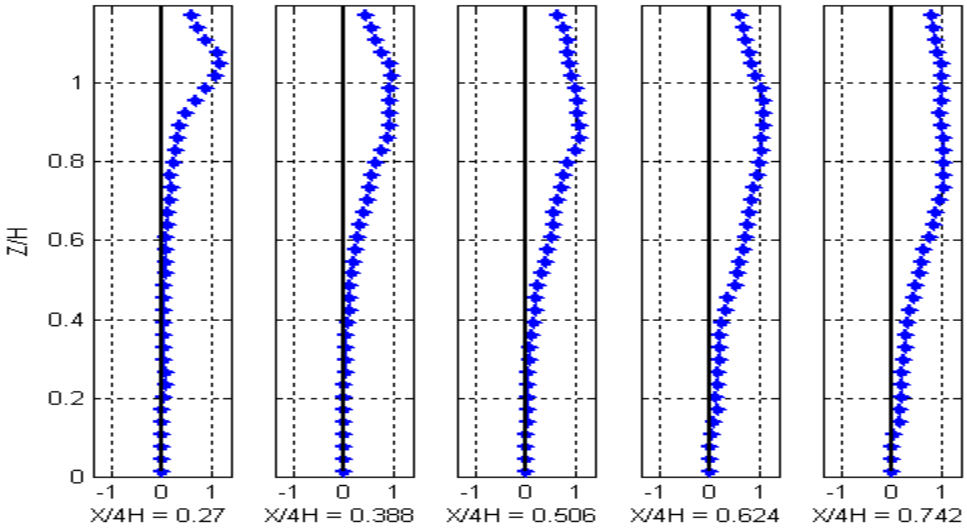

Figure 13 – Profiles of normalized Reynolds Stress ($\overline{u'w'}/\overline{u'w'}_H$) at five equidistant streamwise locations along the center plane of the street canyon for the case x4h_α15_0β.

Note: X/4H is the non dimensional distance of the of the location where the profile has been plotted from the center of the upwind building.

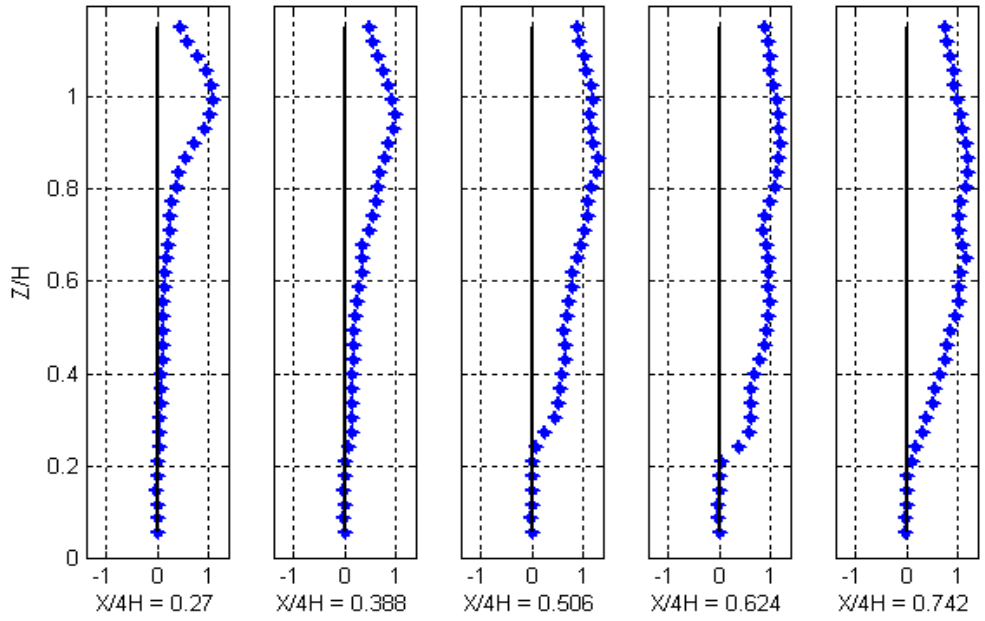

Figure 14 – Profiles of normalized Reynolds Stress ($\overline{u'w'}/\overline{u'w'}_H$) at five equidistant streamwise locations along the center plane of the street canyon for the case x4h_α30_0β.

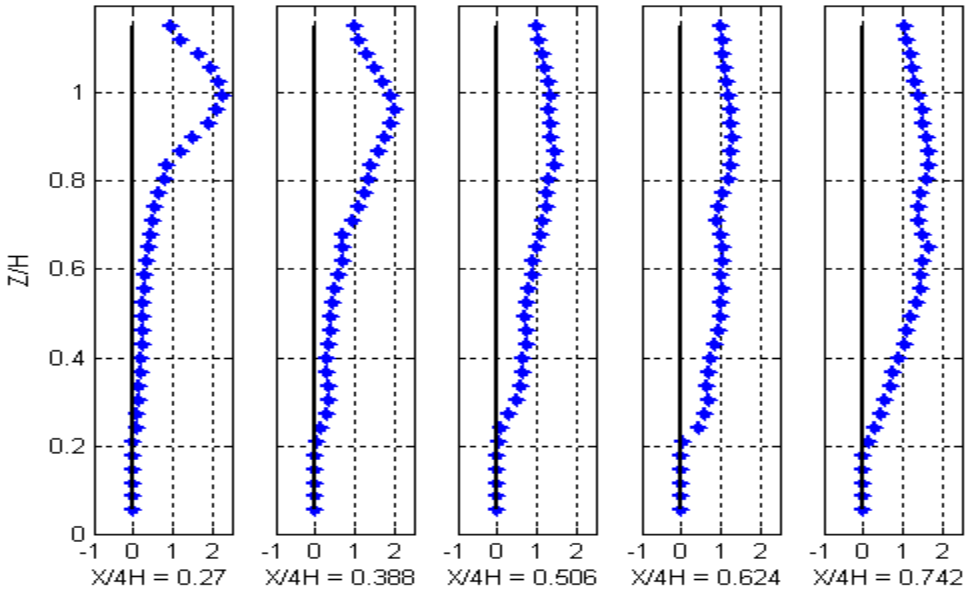

Figure 15 – Profiles of Normalized Reynolds Stress ($\overline{u'w'}/\overline{u'w'}_H$) at five equidistant streamwise locations along the center plane of the street canyon for the case x4h_α45_0β.

Note: X/4H is the non dimensional distance of the of the location where the profile has been plotted from the center of the upwind building

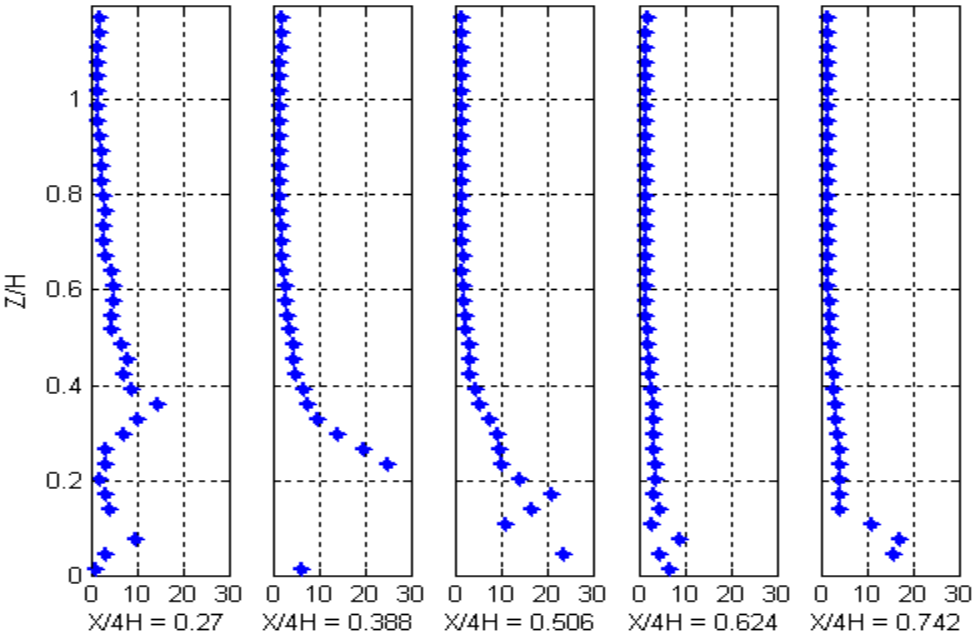

Figure 16 – Profiles of the ratio of TKE/Reynolds stress at five equidistant streamwise locations along the center plane of the street canyon for the x4h_α15_0β case.

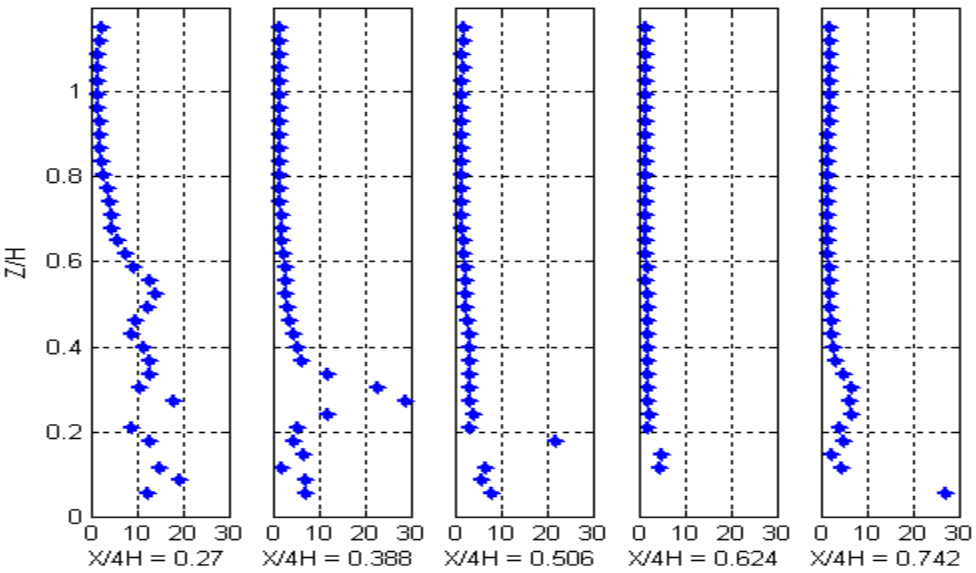

Figure 17 – Profiles of the ratio of TKE/Reynolds stress at five equidistant streamwise locations along the center plane of the street canyon for the x4h_α30_0β case.

Note: X/4H is the non dimensional distance of the of the location where the profile has been plotted from the center of the upwind building

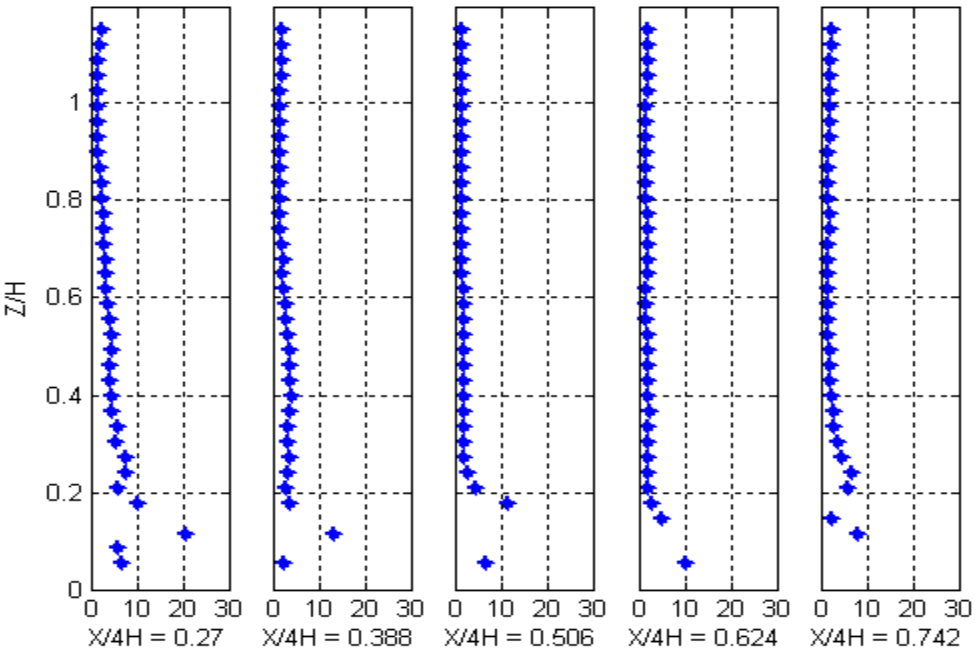

Figure 18 – Profiles of the ratio of TKE/Reynolds stress at five streamwise locations along the center plane of the street canyon for the x4h_α30_0β case.

From the above figures we find that the ratio of TKE / Reynolds Stress is higher for α = 15° when compared to when α = 30 and 45°. This could be attributed to the fact that there is greater diffusion of the Reynolds Stress into the canyon for the cases α = 30 and 45° when compared to the TKE and this phenomenon in evident from figures 8 to 13.

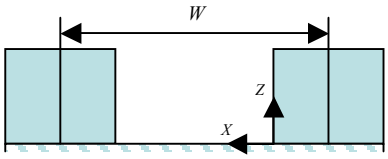

Figure 19 – Schematic showing the coordinate system used for locating the maximum value of TKE.

4. OBSERVATIONS

From the results obtained for the experimental configurations described above, a number of observations regarding the locations of maximum TKE have been made. Since the downwind building was always normal to the upwind flow for these cases, the distance to the location of the maximum value of TKE was obtained by measuring upstream from the upwind face of the downwind building (See Fig below). This distance was then non-dimensionalized by the width of the street canyon x (*W)* (i.e. 4*H* and 3.5*H*) for the configurations being considered. The results for the locations of the maximum TKE are documented as follows. Tables 3 to 5 summarize these observations.

Table 3 – Location of the maximum TKE for the case *W = 4H.*

α	Max TKE (m^2s^{-2})	TKE maximum Location		Non Dimensional Location by *W* (=4*H*) and *H*	
		X (mm)	*Z* (mm)	*X/W*	*Z/H*
15	1.972	67.275	32.131	0.523	1.004
30	2.372	57.234	30.123	0.447	0.94
45	2.513	59.242	31.127	0.462	0.972

Table 4 - Location of the maximum TKE for the case *W = 3.5H.*

α	Max TKE (m^2s^{-2})	TKE maximum Location		Non Dimensional Location by *W* (=3.5*H*) and *H*	
		X (mm)	*Z* (mm)	*X/W*	*Z/H*
15	2.305	35.87	32.1028	0.32	1.003
30	2.397	42.489	32.1012	0.379	1.0032
45	2.301	47.21	31.1586	0.4215	0.973

From the above two tables, the difference in the non-dimensional locations of maximum values of TKE may be obtained by:

$$X^* = (X/W)_{x=4h} - (X/W)_{x=3.5h}$$

$$Z^* = (Z/H)_{x=4h} - (Z/H)_{x=3.5h}$$

Table 5 – Non-dimensional differences in the location of the maximum TKE for the two separation distances considered.

α	Non Dimensional difference for the cases	
	X^*	Z^*
15	0.2025	0.001
30	0.068	-0.0632
45	0.0405	-0.001

The results in Table 5 indicate that the location of maximum TKE is further downstream for the 3.5H case than the 4H case, but that in both cases the maximum is at approximately building height. This can be explained by looking at the streamtraces shown in figures 1 to 8. At 15 ^{o}, the flow in the 4H case is still in a dual co-rotating vortex mode indicative of the wake interference regime, while in the 3.5H case, the flow has transitioned toward skimming flow regime with one single vortex. By 45 ^{o}, both configurations appear to be in a similar skimming mode and the locations of maximum stress are quite similar.

5 CONCLUSIONS

2D Particle Image Velocimetry (PIV) was employed to investigate the flow field in a street canyon with varying building orientations and separation distances. Mean and Turbulence statistics were obtained for the different configurations. The results give an interesting overview of the flow features. It was found that a ratio of less than 0.4 for the building height to the street canyon width does not necessarily result in an 'isolated roughness flow' in the street canyon as is suggested in the work of Hussain and Lee (1980). The experiments performed also confirm the claim of Sini et al (1996) that H/W<0.4 is not a sufficient condition for an isolated flow in the canyon.

It was seen that for a street canyon with width W = x = 4H, as the orientation of the upwind building was increased from 15 to 45°, the vertical component of velocity grew to as much as 40% the value of the velocity at the building height in an uninterrupted boundary layer without the buildings. This finding needs to be investigated more thoroughly in terms of understanding the mechanisms that drive this phenomenon as it could have serious implications on street canyon designs in the future in a real city.

It was also observed that the magnitude of maximum Reynolds stress and TKE increased and shifted downstream the upwind building as the upwind building was rotated.

Further, it was observed that though a change in the angle of the upwind building from 0 to 45° caused only a minor change in the street canyon width for the cases considered, it caused a change in the flow field from a 'wake interference regime' to almost the 'skimming flow regime'. This behavior due to a change in the orientation of the upwind building could be better understood if the velocity information of the spanwise component was available.

The present paper opens up interesting avenues for further research to understand the effect of the change in the upwind building orientation on the coupling of the vortices, change in the location of maximum TKE and Reynolds stress and myriads of other aspects associated with the flow field. Consequently, future work would involve taking measurements in the plan view or taking stereoscopic PIV measurements to get a picture of the whole field in the street canyon for the above considered configurations.

REFERENCES

Xueling C., and H. Fei, 2005: Numerical Studies on flow fields around buildings in an urban street canyon and cross-road. *Advances in Atmospheric Sciences,* **22**, 290-299

Hotchkiss, R.S., F.H. Harlow, 1973: Air

pollution in street canyons. EPA-R4-73-029

Hoydysh, W.G., W.F. Dabberdt, 1988: Kinematics and dispersion characteristics of flows in asymmetric street canyons. *Atmospheric Environment*, **12**, 2677-2689.

Hunter, L., G.T. Johnson, I.D. Watson, 1992: An investigation of three-dimensional characteristics of flow regimes within the urban canyon.. *Atmospheric Environment*, **7**, 425-432.

Hussain, M., and B.E. Lee 1980: The influence of wind forces on 3-D roughness elements in a simulated atmospheric boundary layer flow. Part II – flow over large arrays of identical roughness elements and the effect of frontal and side aspect ratio variations. Department of Building Sciences, Univiversity of Sheffield, U.K

Baik, J.-J., and Kim, J.-J., 1998: A Numerical Study of flow and Pollutant Dispersion Characteristics in Urban Street Canyons. *J. Appl. Meteor*., **38,** 1576-1589.

Kastner-Klein, P., R. Berkowicz, and R. Britter, 2004: The influence of street architecture on flow and dispersion in street canyons. *Meteorol. Atmos. Phys,* **87***,* 121-131.

Kastner-Klein, P., and M.W. Rotach, 2004: Mean Flow and turbulence characteristics in an urban roughness sub layer. *Boundary-Layer Meteorology*, **111**, 55-84.

Louka, P., S.E. Belcher, and R.G. Harrison, 1998: Modified Street Canyon flow. *J. Wind Eng. Ind. Aerodyn,* **74-76**, 485-493.

Oke, T.R., 1988: Street design and urban canopy layer climate. Energy and Building, **11**, 103-113.

Arya, P.S., 1988: Introduction to Micrometreology. Academic press, New York.

Sini, J.F., S. Anquetin, and P.G. Mestayre, 1996: Pollutant Dispersion and Thermal Effects in Urban Street Canyons. *Atmospheric Environment*, **30**, 2659-2677

Snyder, W.H., and R.E. Lawson, 1994: Wind-tunnel measurements of flow fields in the vicinity of buildings. *8th Joint Conf. on Applic. of Air Poll. Meteor. With AWMA*, Nashville, TN, Amer. Meteor. Soc., 23-28.

Thanh Ca, V., A. Takashi, I. Manabu, and S. Armfield, 1995: Characteristics of wind field in a street canyon. *J. Wind Eng. Ind. Aerodyn*, **57,** 63-80